AUTO-COMBUSTION SYNTHESIS OF Al-DOPED ZnO NANOPARTICLES: STRUCTURAL AND ENERGY BAND GAP ENHANCEMENT

M.S.M. Suan[1], I.M. Yusof[1] and I. Nurdin[2]

[1]Faculty of Manufacturing Engineering,
Universiti Teknikal Malaysia Melaka, Hang Tuah Jaya, 76100 Durian Tunggal, Melaka, Malaysia.

[2]Department of Chemical Engineering,
Lhokseumawe State Polytechnic, 24301
Aceh, Indonesia.

Corresponding Author's Email: [1]mohdshahadan@utem.edu.my

Article History: Received 19 October 2019; Revised 19 March 2020; Accepted 20 October 2020

ABSTRACT: Auto-combustion reaction has been developed as a new route in synthesizing ZnO and Al-doped ZnO nanoparticles with improved structural, and optical properties. In this work, the effects of Al doping concentrations and different calcination temperatures were investigated. The $Zn(NO_3)_2$ aqueous solution was mixed with $Al(NO_3)_3$, citric acid, and ammonia aqueous solutions to obtain a series of mixtures with varied Al molarity concentration, x from 0 to 0.5. The highly exothermic single-step auto-combustion reaction at around 230 °C has transformed the mixture into fine black ashes which yielded white powder during calcinated at various calcination temperature, T_{cal} for 1 h in a normal furnace atmosphere. The XRD results revealed that the transformation of amorphous ZnO ashes into highly crystalline ZnO with a hexagonal structure was completed at $T_{cal} \geq 700$ °C where the c lattice constant in the samples was increased by the increases of Al doping concentration. The SEM images of the $Zn_{1-x}Al_xO$ samples calcined at $T_{cal} = 700$ °C showed a dense and highly packed of ZnO nanoparticles due to the increased of Al diffusion in ZnO and higher grain growth rate of ZnO. The energy band gap obtained from UV-vis results was significantly improved in $Zn_{1-x}Al_xO$ samples calcined at $T_{cal} = 700$ °C attributed to the well-controlled of Al doping concentration in effectively adjusting the electronic properties of the ZnO nanoparticles.

KEYWORDS: *Al-Doped ZnO; Nanoparticles; Auto-Combustion; Calcination; Energy Band Gap*

1.0 INTRODUCTION

Research on zinc oxide (ZnO) nanoparticles has been revived and rapidly expands in these recent years. The high electron mobility, high thermal conductivity, wide and direct band gap, and large excitation energy made the ZnO nanoparticles suitable for various range of devices, including gas sensors, dielectric for electronic materials, and energy conversion and storage [1-3]. Despite the rapid developments, controlling structural and optical stabilities of ZnO nanoparticles remain a major challenge due to degradation of these properties in the ambient environment [4-5]. Javed et al. [6] reported that the stabilities, electronic, and photocatalytic properties of ZnO can be increased through the doping of group III elements include B, In, Ga, and Al. Among these elements, Al is an interesting and effective element to be doped into ZnO because of its comparable atomic radius with the Zn. Although there are many reports on the doping of Al in the ZnO, the work on obtaining the nanoparticles of this compound was still insufficient due to the restriction of the current synthesis methods such as solid-state processing [7], precipitation [8], and hydrothermal process [9] which has resulted with non-uniform distribution and existence of impurities.

Therefore, the synthesizing method is crucial in order to achieve the accurate, and homogeneous concentration of Al in ZnO nanoparticles. The auto-combustion reaction attracted much attention because of it has successfully been used in synthesizing various highly pure ceramic oxides with well-controlled of the concentration includes Al_2O_3, $YBa_2Cu_3O_{7-\delta}$, Al doped YBCO, ZrO_2 and TiO_2 [10-12]. Thus, in this work, Al was doped within ZnO through an auto combustion reaction as a novel technique to obtain highly pure of Al-doped ZnO nanoparticles. The calcination process afterward provides thermal and structural stability to the nanoparticles was reported to greatly influence the properties of the nanoparticles. Thus, the effects of calcination temperatures were investigated in order to enhance structural, and optical properties of Al-doped ZnO nanoparticles.

2.0 METHODOLOGY

Aqueous solutions of $Zn(NO_3)_2$ (0.5 M) and $Al(NO_3)_3$ (0.5 M) have been mixed by varying the Al molarity concentration, x where x = 0.1, 0.5 and 0.0 for the undoped ZnO. The mixtures were complexed with citric acid solution (0.5 M) by the citrate to nitrate ratio = 0.6 and their pH was adjusted to pH≈7 by adding liquor ammonia. The as-prepared mixture

was dried on the hot plate at 250 °C while the infrared lamp has been used to provide uniform heating from the top. In the drying process, the mixture has been changed into the gel before automatically combusted into ashes. In order to investigate the effects of T_{cal} on the nanoparticle's properties, the resultant ashes have been calcined at 600, 700, and 800°C for 1 hour in ambient atmosphere and cooled in the furnace while the un-calcined ashes will be the control sample. The calcination has changed the black ashes into the white powder. The X-ray diffraction (XRD) for the calcined powder phase identification and crystallite size estimation was carried out using Ni-filtered Co Kα radiation by Bruker D8-advanced XRD machine. The peak position and intensities were obtained between 20° and 80° with a velocity of 0.02° s^{-1}.

Scanning electron microscope (SEM) Zeiss Ultra 40XB was used to observe the sample's microstructure. While, Shimadzu 1700 UV-Vis spectrophotometer was used to study the optical absorption of the zinc oxide nanoparticles. The bandgap energy was calculated from the absorption spectrum by using Tauc equation; $\alpha = [A(h\upsilon - E_g)^{n/2}]/h\upsilon$, where α is absorbance, A is a constant between 10^7 and 10^8 m^{-1}, E_g is the band gap energy that occupies the area between the bottom of the conduction band and the top of the valence band and K and n is the constant that equal to 1 and 4 for direct band gap and indirect band gap respectively υ is the frequency, h is the Planck's constant.

3.0 RESULTS AND DISCUSSION

Thermal behaviors of the gel samples throughout the combustion reaction represented by the TG and DTA curves are shown in Figure 1. Analysis on these curves revealed that each gel samples decomposed by a rapid decomposition behavior where the gel samples undergo a minor mass lost followed by a major loss of mass (>40 wt. %) in a single exothermic reaction at ~ 230 °C and thermally stable after 400 °C. It also can be seen that, by the increase of Al concentration, the exothermic peak on the DTA curves is shifted to the lower temperature with the appearance of low intense exothermic peaks. The minor loss of mass at around 100 °C to 200 °C is due to the removal of excesses water and decomposition of citric acid. As the temperature increases, citric acid ($C_6H_8O_7$) began to decompose to aconitic acid ($C_6H_6O_6$) at 183 °C [13]. Upon continuous heating, aconitic acid is further decomposed to itaconic acid ($C_5H_6O_4$) which acted as the fuel once for this combustion. Alongside, the reaction between $Zn(NO_3)_2$ and $Al(NO_3)_3$ with ammonia solution has formed Zn hydroxide, Al hydroxide, and ammonium nitrate. Once ignited by the pyrolysis of ammonia nitrate, itaconic acid

will be combusted where the heat energy that released from the combustion is enough to remove the water from the Zn hydroxide and Al hydroxide to form ZnO and AlO respectively. In the Al-doped samples, decomposition of $Al(NO_3)_3$ occurred earlier than the decomposition of $Zn(NO_3)_2$ [14]. The combustion emitted a large amount of carbon dioxide (CO_2) and nitrogen (N_2) gases. The overall decomposition reaction is shown in Equation (1).

$$Zn(NO_3)_2 + \boldsymbol{x}Al(NO_3)_3 + 5C_6H_7O_8 \rightarrow 9ZnO + \boldsymbol{x}AlO + 20H_2O + 30CO_2 + 9N_2 \quad (1)$$

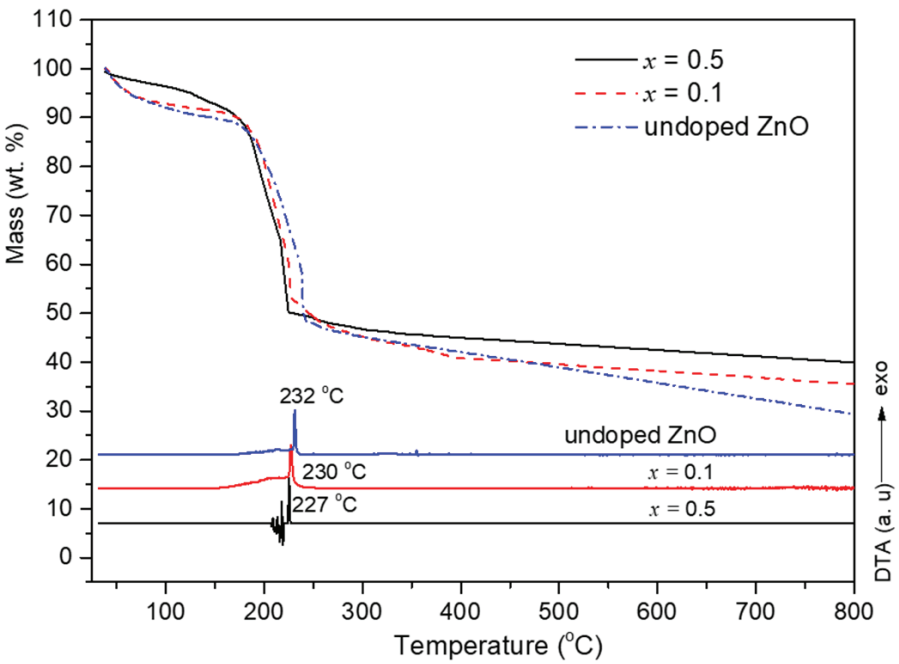

Figure 1: TG/DTA curves of precursor gels with different Al concentration

Figure 2 shows the XRD patterns of the ZnO powder samples after calcinated at different temperatures. It can be found that the samples calcined at Tcal ≥ 700 °C yielded high crystallinity of pure ZnO since all peaks with high intensity occurred at the same Bragg diffraction angles of the ZnO (JCPDS card No. 00-036- 1451). The significant peaks detected on the patterns were assigned to (100), (002), (101), (102), (110), and (103) planes of the wurtzite structure ZnO [15]. While the XRD pattern of the sample calcined at 600 °C showed a lower intensity of ZnO peaks with the existence of impurities. In this occasion, it can be suggested that the volatile matters and impurities in the ashes as indicated by XRD pattern of the un-calcined sample were vaporized during the calcination process.

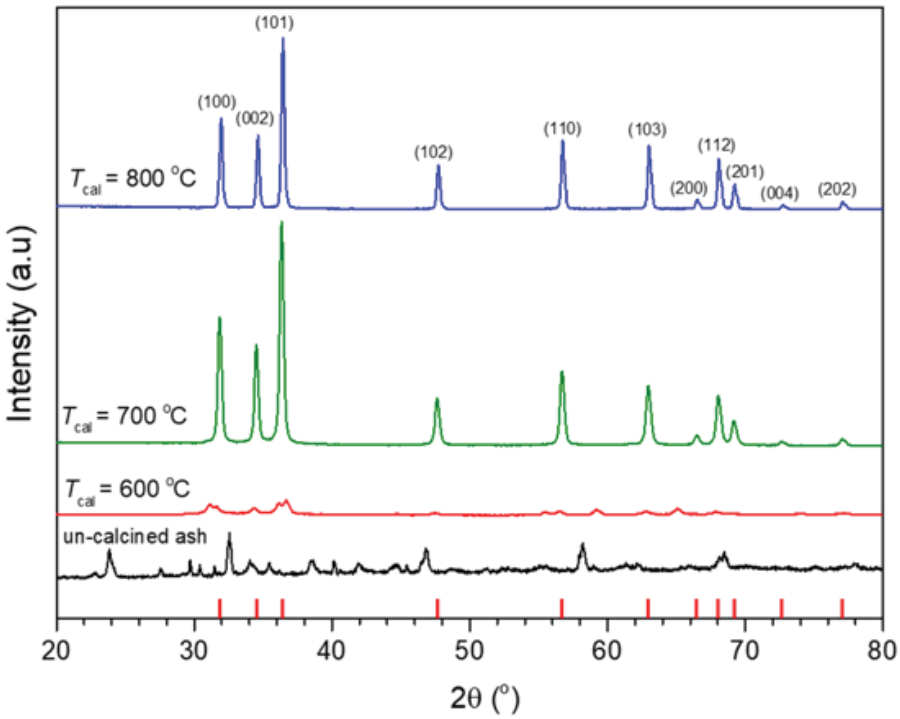

Figure 2: XRD patterns of the pure ZnO and Al-doped ZnO samples calcinated at different temperatures

The calcination at temperature ≥700 °C is required to complete the vaporization process although the TG analysis showed the ashes were stable after 400 °C. It also been revealed that the amorphous ZnO in the ashes obtain enough energy to transform into crystal ZnO at Tcal ≥700 °C as shown by the reaction in Equation (2).

$$\text{ZnO (amorphous)} \rightarrow \text{ZnO (crystalline)} \quad (2)$$

Figure 3 shows the XRD pattern of pure ZnO and Al doped ZnO samples with different Al doping concentration x after calcinated at T_{cal} = 700 °C. The patterns which is most likely similar with the samples calcined at T_{cal} = 800 °C are indicated to the polycrystalline ZnO as the significant peaks have existed at the same Bragg diffraction angles of the wurtzite structure ZnO. There is no peak assigned to Al was detected on the Al doped ZnO patterns due to relatively small doping concentration of Al. However, the presence of Al in the samples has been confirmed by EDX analysis as listed in Table 1. Include in the table is the variation of crystallite sizes and lattice parameters of the samples calcined at $T_{cal} \geq 700$ °C.

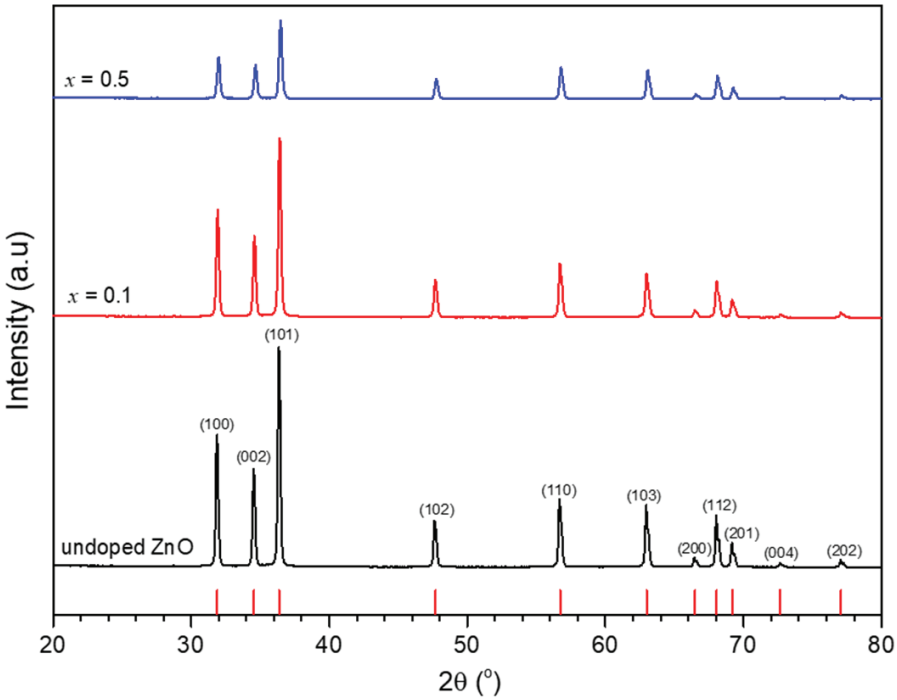

Figure 3: XRD pattern of pure ZnO and Al doped ZnO samples with different x calcinated at T_{cal} = 700 °C

The elemental analysis listed in Table 1 shows the presence of Al in Al doped samples. The atomic percentage of Zn, Al, and O in each sample have achieved the expected theoretical formulation which indicates the effectiveness of this synthesis method in controlling the composition of the compound. Table 1 also lists the crystallite size and lattice parameters of the ZnO and Al doped ZnO samples with different x calcined at T_{cal} = 700 °C and 800 °C. The crystallite size of each sample synthesized by using auto-combustion reaction is in the range from 48 to 68 nm. It can be found that the crystallite size of samples is increased by the increase of T_{cal} and Al doping concentration. This phenomenon is attributed to the increase of the grain growth rate and substitution of Al^{+} in the ZnO crystal, respectively [16]. The lattice constants of undoped ZnO sample (x = 0.0) is slightly increased with the increased of T_{cal} which have been reported due to oxygen deficiency [17]. While in Al doped samples, incorporation of Al^{+} in ZnO crystal has altered the c lattice constant. The Al+ ion is favorably to partially replace at Zn+ ion. The incorporation becomes more significant at higher x and T_{cal}.

However, the c lattice constant of the samples with x = 0.5 calcined at T_{cal} = 800 °C (5.1877 Å) has found to be lower than T_{cal} = 700 °C (5.1893 Å). There is a possibility where the Al^{+} has transformed into Al_2O_3 at higher calcination temperature as reported by Suan and Johan [14], hence lower the amount of incorporation Al^{+} in ZnO crystal. The c/a ratio which indicates the hexagonal structure of ZnO of each sample remains unchanged at around 1.6 in each sample.

Table 1: Lattice parameters and elemental analysis of ZnO and Al-doped added ZnO samples

T_{cal} (°C)	x	EDX of grain (At. %)			Expected Formula	Crystallite size (nm)	Lattice Constant (Å)		
		Zn	Al	O			a	c	c/a
700	0.0	51.32	-	48.66	ZnO	48.8	3.2377	5.1811	1.6002
700	0.1	41.63	10.85	47.32	$Zn_{0.9}Al_{0.1}O$	49.2	3.2399	5.1823	1.5995
700	0.5	28.32	25.92	47.57	$Zn_{0.5}Al_{0.5}O$	52.3	3.2481	5.1893	1.5976
800	0.0	50.74	-	49.23	ZnO	58.7	3.2378	5.1815	1.6003
800	0.1	40.05	10.13	48.40	$Zn_{0.9}Al_{0.1}O$	64.5	3.2440	5.1834	1.5978
800	0.5	25.76	25.15	48.13	$Zn_{0.5}Al_{0.5}O$	67.1	3.2482	5.1877	1.5970

Figure 4 shows the microstructure of ZnO and Al doped ZnO samples calcinated at 700 °C and 800 °C. It can be observed in Figure 4 (a), the pure ZnO sample has existed as distinctive and spherical shape particles with the uniform size around 100 nm. While in Figure 4 (c), the presence of Al in the ZnO particles have resulted with broader range of particle size from 50 to 200 nm. Both samples were growing into the larger and denser microstructure by the increased of calcination temperature as shown in Figures 4 (b) and (d) respectively. The occurrence of Al is significant in Al doped ZnO sample with x = 0.5. The microstructure of this sample is observed to be denser and larger compare to the other compositions. The samples yielded into molten-like microstructure after calcinated at 800 °C as depicted in Figure 4 (f). This can be attributed to the excesses Al which has melted and filled in the inter-boundary pores during the calcination process. At the higher calcination temperature, the grain growth rate of the sample was enhanced hence resulted with larger microstructure.

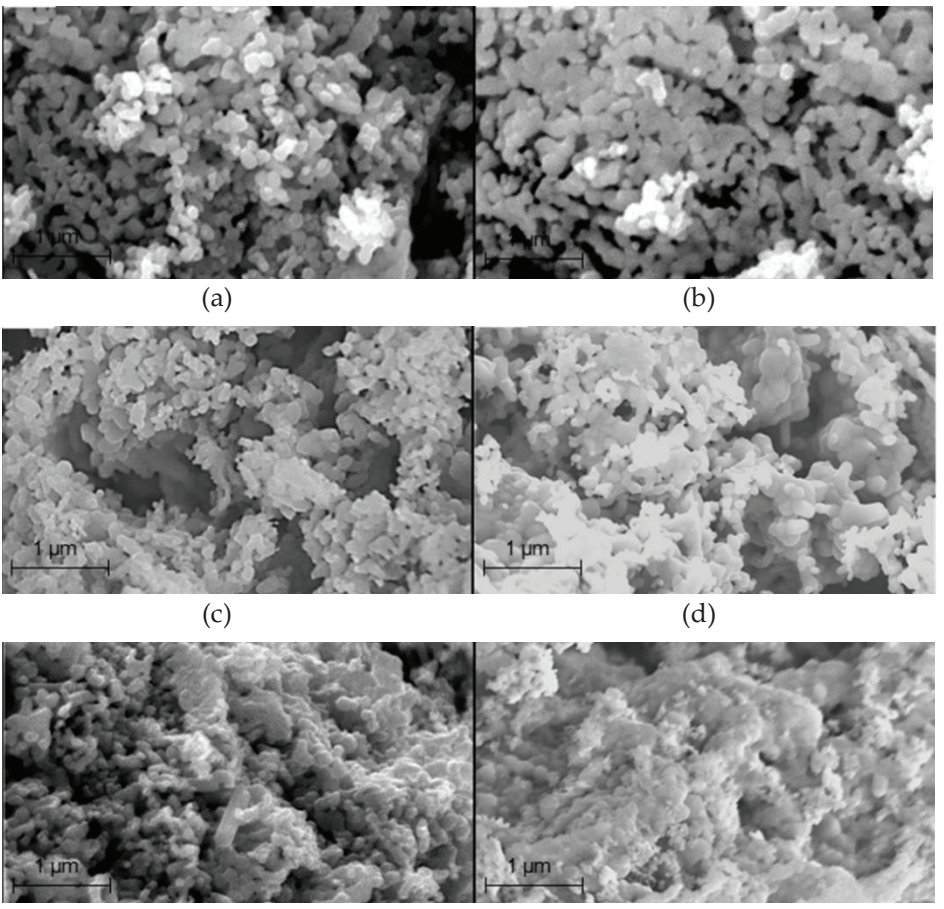

(a) (b)

(c) (d)

(e) (f)

Figure 4: SEM images of ZnO and Al doped ZnO samples calcinated at 700 °C and 800 °C of (a) pure ZnO, T_{cal} =700 °C, (b) pure ZnO, T_{cal} =800 °C, (c) x=0.1, T_{cal} =700 °C, (d) x=0.1, T_{cal} =800 °C, (e) x=0.5, T_{cal} =700 °C and (f) x=0.5, T_{cal} =800 °C

Figure 5 shows the energy band gap of the pure ZnO and Al doped ZnO calcinated at different temperatures. It can be clearly seen that the energy band gap is maximized in the samples calcinated at 700 °C where the maximum value of 3.292 eV is obtained in the sample with x = 0.5. The value is improved as compared with the study by Kamarulzaman et al. [18]. However, the energy band gap of this sample was dropped to 3.286 eV as the calcination temperature was increased to 800 °C. As for the pure ZnO and Al doped ZnO with x = 0.1 samples, the value is stabilized at around 3.288 eV and 3.289 eV at 700 and 800 °C respectively. This phenomenon can be related to the structural properties of the ZnO and the role of Al as the efficient doping element.

At T_{cal} < 700 °C, the ZnO is existed with narrow energy band gap attributed to lower crystallinity. The doping of Al did not bring to much improvement because the Al at this T_{cal} showed lower tendency to diffuse in and alter the ZnO structure. The intrinsic transition between conduction band and valence band triggered by Al in Al-doped ZnO crystal is optimized at T_{cal} = 700 °C. The ZnO is highly crystalline where the better control of Al doping concentration has further widened the band gap. While at T_{cal} > 700 °C, Al tend to be transformed into Al oxide which lowered its role to improve the band gap.

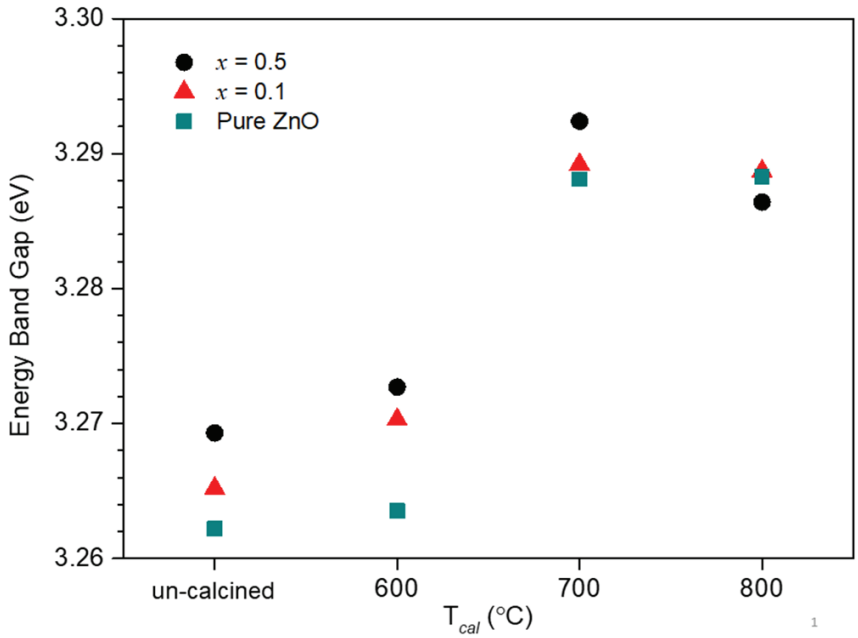

Figure 5: Energy band gap of the pure ZnO and Al doped ZnO calcinated at different temperatures

4.0 CONCLUSION

Auto-combustion reaction at 230 °C followed by the calcination process at temperature ≥ 700 °C has successfully yielded wurtzite structure of polycrystalline $Zn_{1-x}Al_xO$ with the c/a lattice ratio and particles size around 1.6 and 100 nm respectively. The energy band gap of ZnO was enhanced attributed incorporation of Al to form $Zn_{1-x}Al_xO$ compound at 700 °C. At the T_{cal} = 800 °C, excesses of Al in sample with x = 0.5 has formed Al_2O_3 at the inter-grain boundaries of ZnAlO hence improved the microhardness of the sample.

ACKNOWLEDGMENTS

The authors gratefully acknowledge to Universiti Teknikal Malaysia Melaka for the facilities and also everyone who contributed in giving the helpful suggestions and comments.

REFERENCES

[1] D.R. Miller, S.A. Akbar, and P.A. Morris, "Nanoscale metal oxide-based heterojunctions for gas sensing: A review", *Sensors and Actuators B: Chemical*, vol. 204, pp. 250-272, 2014.

[2] S. Park, C.H. Kim, W.J. Lee, S. Sung, and M.H. Yoon, "Sol-gel metal oxide dielectrics for all-solution-processed electronics", *Materials Science and Engineering: R: Reports*, vol. 114, pp. 1-22, 2017.

[3] O. Edynoor, A. Warikh, T. Moriga, K. Murai, E. Mohammad, and M. Salleh, "Effect of Annealing Time on Resistivity of Kenaf Fiber Modified Indium Zinc Oxide Prepared Via Dip Coating Process", *Journal of Advanced Manufacturing Technology*, vol. 11, no. 1(1), pp. 139-150, 2017.

[4] S. Repp, and E. Erdem, "Controlling the exciton energy of zinc oxide (ZnO) quantum dots by changing the confinement conditions", *Spectrochimica Acta-part A: Molecular and Biomolecule Spectroscopy*, vol. 152, pp. 637-644, 2016.

[5] D. Segets, J. Gradl, R. K. Taylor, V. Vassilev and W. Peukert, "Analysis of optical absorbance spectra for the determination of ZnO nanoparticle size distribution, solubility, and surface energy", *ACS Nano*, vol. 3, no. 7, pp. 1703-1710, 2009.

[6] R. Javed, M. Usman, S. Tabassum and M. Zia, "Effect of capping agents: Structural, optical and biological properties of ZnO nanoparticles", *Applied Surface Sciences*, vol. 386, pp. 319-326, 2016.

[7] Z.P. Sun, L. Liu, L. Zhang and J. Dian-Zeng, "Rapid synthesis of ZnO nano-rods by one-step, room-temperature, solid-state reaction and their gas-sensing properties", *Nanotechnology*, vol. 17, no. 9, pp. 2266-2270, 2006.

[8] D. Raoufi, "Synthesis and microstructural properties of ZnO nanoparticles prepared by precipitation method", *Renewable Energy*, vol. 50, pp. 932-937, 2013.

[9] S. Kumar and P.D. Sahare, "Observation of band gap and surface defects of ZnO nanoparticles synthesized via hydrothermal route at different reaction temperature", *Optics Communication*, vol. 285, no. 24, pp. 5210-5216, 2012.

[10] J. Li, Y. Wu, Y. Pan, W. Liu, Y. Zhu and J. Guo, "Influence of citrate-to-nitrate ratio on the thermal behavior and chemical environment of alumina gel", *Ceramics International*, vol. 33, no. 5, pp. 1539 -1542, 2008.

[11] K.A. Singh, L.C. Pathak and S.K. Roy, "Effect of citric acid on the synthesis of nano-crystalline yttria stabilized zirconia powders by nitrate–citrate process", *Ceramics International*, vol. 33, no. 8, pp. 1463-1468, 2007.

[12] S. Tabesh, F. Davar, and M. R. Loghman-Estarki, "Preparation of γ-Al_2O_3 nanoparticles using modified sol-gel method and its use for the adsorption of lead and cadmium ions", *Journal of Alloys and Compounds*, vol. 730, pp. 441-449, 2018.

[13] S. Banerjee and P.S. Devi, "Effect of citrate to nitrate ratio on the decomposition characteristics and phase formation of alumina", *Journal of Thermal Analysis and Calorimetry*, vol. 90, no. 3, pp. 699-706, 2007.

[14] M.S.M Suan, and M.R. Johan "Synthesis of $Y_{1-x}Al_xBa_2Cu_3O_{7-\delta}$ via combustion route: Effects of Al_2O_3 nanoparticles on superconducting properties", *Physica B: Condensed Matter*, vol. 506, pp. 178-182, 2017.

[15] Z.N. Kayani, F. Saleemi and I. Batool, "Synthesis and characterization of ZnO nanoparticles", *Materials Today: Proceedings*, vol. 2, no. 10, pp. 5619-5621, 2015.

[16] M.Chitra, K. Uthayarani, N. Rajasekaran and E.K. Girija, "Preparation and Characterisation of Al doped ZnO Nanopowders", *Physics Procedia*, vol. 49, pp. 177-182, 2013.

[17] J. Wang, R. Chen, L. Xiang and S. Komarneni, "Synthesis, properties and applications of ZnO nanomaterials with oxygen vacancies: A review", *Ceramics International*, vol. 44, no. 7, pp. 7357-7377, 2018.

[18] N. Kamarulzaman, M.F. Kasim, and R. Rusdi, "Band gap narrowing and widening of ZnO nanostructures and doped materials", *Nanoscale Research Letters*, vol. 10, no. 1, pp. 1-12, 2015.